Electronic Supplementary Material (ESI) for Nanoscale
This journal is © The Royal Society of Chemistry 2012

Supporting Information

All Inorganic Iron Pyrite Nano-Heterojunction Solar Cells

Alec Kirkeminde, Randall Scott and Shenqiang Ren[*]

Department of Chemistry, University of Kansas, Lawrence, Kansas 66045, United States

1. Methods

1.1. Synthesis of FeS_2 Nanocubes and CdS Quantum Dots

The FeS_2 NCs were synthesized by injection of excess sulfur into decomposed metal precursor ($FeCl_2$) followed by growth, then the second injection of $FeCl_2$. All synthesis was done under Argon atmosphere using standard Schlenk line techniques. In one flask, 4 mmol elemental sulfur was dissolved in 5 mL diphenyl ether and sonicated untill all sulfur was dissolved and then degassed for one hour at 70 ^oC under argon. In a separate vessel 0.5 mmol of $FeCl_2$ is dissolved in 12 g Octadecylamine (ODA) and degassed for 1 hour at 120 ^oC to allow for decomposition. The iron solution is then raised to 220 ^oC and the sulfur solution was rapidly injected into the iron solution. The solution immediately turned black upon injection. This solution was allowed to react for 90 min. During this time, another vessel was prepared with 0.125 mmol $FeCl_2$ and 4 g ODA and allowed to decompose at 120 ^oC under argon. At 90 min, 1 mL of the second iron solution was rapidly injected into the flask. This solution was kept at 220 ^oC and allowed to react for another 90 min. Aliquots were taken at different times to access growth. After the reaction was finished, the solution was allowed to cool to ~100 ^oC and halted with injection of methanol and crashed out using the centrifugation. The NCs were cleaned up using standard crash out/wash method using chlorophorm/ethanol by the centrifugation in a N_2 glovebox. After cleaning the NCs were redispersed in chloroform for storage and characterization.

CdS quantum dots (QDs) were synthesized following reports by Peng *et al.*[1] Cadmium precursors were prepared by dissolving 514 mg of cadmium oxide in a mixture of 20 mL of oleic acid and 150 mL of 1-octadecene at 160 °C under argon flow and degassing at 100 °C under vacuum. The temperature of the precursor solution was then raised to 300 °C under argon flow for 30 min and then cooled to 100 °C for further degassing. The degassed cadmium precursor solution was again heated to 300 °C followed by swift injection of degassed sulfur precursors formed with 64 mg of sulfur powder and 20 mL of 1-octadecene. The solution was then held at 280 °C for 12 min before cooling to room temperature. After synthesis, quantum dots were centrifuged and precipitated with isopropanol and then redispersed in hexane. This step was repeated three times prior to n-butylamine ligand exchange. Precipitated CdS QDs were re-dissolved in n-butylamine

This journal is © The Royal Society of Chemistry 2012

and magnetically stirred overnight. After ligand exchange, acetone was used to precipitate CdS QDs, and the final product was re-dissolved in the octane.

1.2. Device Fabrication

All manipulations were performed using standard air-free nitrogen glovebox techniques. The whole device structure consists of the following sequence of films and thicknesses: ITO/poly(3,4-ethylenedioxythiophene):poly(styrenesulfonate) (PEDOT:PSS)(40 nm)/ TFB(10 nm)/FeS_2: CdS (500 nm)/Ca (10 nm)/Al (100 nm). PEDOT:PSS (Baytron PVP CH 8000) is spin cast onto a 0.5 × 0.5 in^2 glass substrate with pre-patterned ITO electrodes. The PEDOT: PSS and TFB layers are useful as a hole transport and smoothes the ITO surface. The resulted FeS_2 NCs in chloroform solution with different ratio concentrations were blended with CdS QDs in the octane solution. The blended solution is spun at 600 rpm for three times, dipped in the sequence of 0.002 M EDT, 0.002 M Hydrazine, and 0.002 M EDT solutions for 30 s, and allowed to solvent annealing overnight. The coated device was annealed at 175°C for 10 min, and then quickly cooled to room temperature. The 10 nm thick Ca layer was evaporated at a rate of 0.1 nm/s as exciton blocking layer, which is followed by top contact Al layer. The top Al contact was evaporated through a shadow mask to generate an array of patterned electrodes. The final device area was defined by the overlap between the top and bottom electrodes.

1.3. Device Characterization

Current-voltage (*J-V*) characteristics of the finished devices are measured in a nitrogen atmosphere glovebox with a source-meter (Keithley 6487). The light response was measured under illumination from a 100mW/cm^2 AM1.5 solar simulator. Transmittance and absorbance spectra of the device active layer were measured with a Shimadzu UV-Vis-NIR dual-beam spectrophotometer (UV-3200). Photoluminescence was performed on a Cary Eclipse fluorescence spectrometer equipped with a xenon flash lamp. Near IR light was provided from a xenon light with near IR filter.

1.4. Structural Characterization

A FEI FEG analytical electron microscope operated at 200 kV was used for transmission electron microscopy (TEM). Elemental mapping was performed using energy-dispersive X-ray spectroscopy (EDS) in conjunction with a TEM operating in STEM mode. For SEM cross-sectional specimen preparation from a complete FeS_2/CdS device, the Si substrate was used instead of the glass substrate to avoid the charging issue, using a Leo 1550 SEM System. High-powered Bruker MicroSTAR high-brilliance microfocus Cu rotating anode X-ray generator was used for x-ray diffraction study. Surface morphology of the devices was investigated using a Digital Instruments Dimension 3000 atomic force microscope (AFM) operating in contact mode.

2. Structure Characterization of FeS_2 NCs

The SEM image in Figure S1 obtained from FeS_2 nanocubes confirmed the size distribution for 90 min aging time. The crystal structure of the FeS_2 nanocubes was monitored by high-powered Bruker MicroSTAR high-brilliance microfocus Cu rotating anode X-ray generator. The phase of FeS_2 nanocubes are identified as the pyrite structure, and the second phase belongs to the surface oxidized state of FeS_2 nanocube due to the long-time drying and exposure in the air to achieve the powder form for the XRD measurement. The FeS_2 based solar cell device fabrication is carried in the N_2 glovebox entirely from the device processing to photovoltaic testing, which avoid the potential oxidation of FeS_2 nanocubes to degrade their optoelectronic properties.

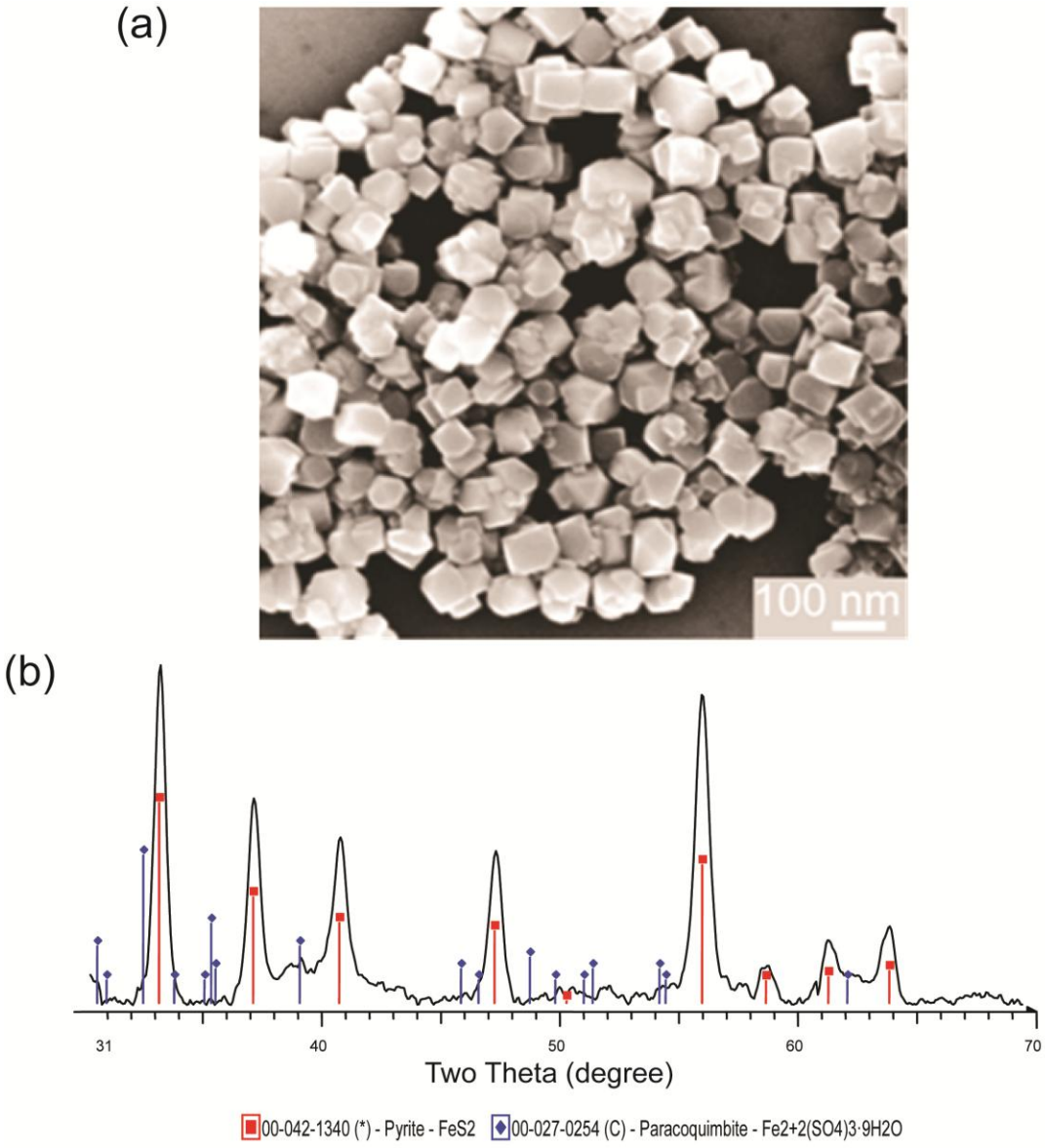

Figure S1. (a) The SEM image of FeS_2 nanocubes for 90 min aging after the second injection. (b) X-ray diffraction patterns of the FeS_2 nanocubes, which confirm the pyrite structures. It can be seen that there is a small amount impurity phase in the XRD which is believed to be an oxidative phase of FeS_2 due to samples being tested in air.

3. UV-vis-NIR Photoabsorption Characterization of FeS_2 NCs and QDs

The optical properties of the FeS_2 NCs and QDs have been studied by UV−vis-NIR absorption spectroscopy (Figure s2). The plot of $(\alpha h\nu)^2$, the square of the absorption coefficient (α) multiplied by the photon energy ($h\nu$) versus $h\nu$ (Figure s2a and s2b), shows a direct band gap of 1.1-1.2 eV which is larger than the reported bulk value (0.89 eV), suggesting the presence of a quantum confinement in band structure due to size or strain effect.[2] Notably, such an increase in band gap is also consistent with the previous reports on FeS_2 nanocrystals as well. [3]

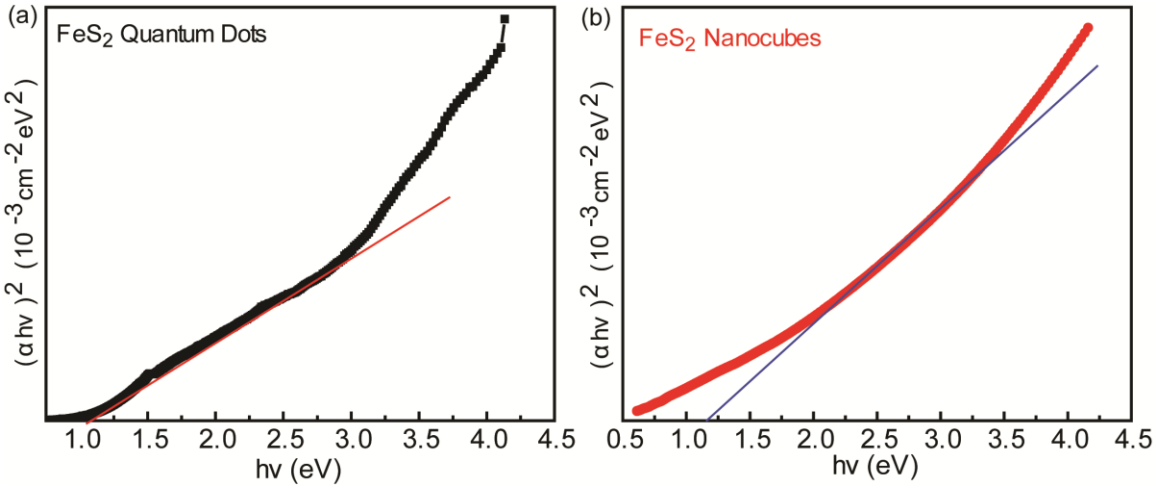

Figure S2. (a) and (b) UV−vis-NIR absorption spectrum of FeS_2 QDs and NCs, respectively. The plot of $(\alpha h\nu)^2$ versus $h\nu$ shows a direct band gap of 1.1-1.2 eV.

4. J-V Characterization of FeS_2:CdS BHJ PV Devices at Different Thickness

Figure S3 shows the thickness dependent *J-V* characteristics of FeS_2:CdS BHJ PV devices. The 250 nm thickness photoactive layer has a larger surface roughness, as shown in the Figure S3a, which reduces the PV performance. By increasing the deposition number and thus the thickness of photoactive layer to 500 nm, we observe that the device exhibits the PCE approximately three times higher than that of the thin device.

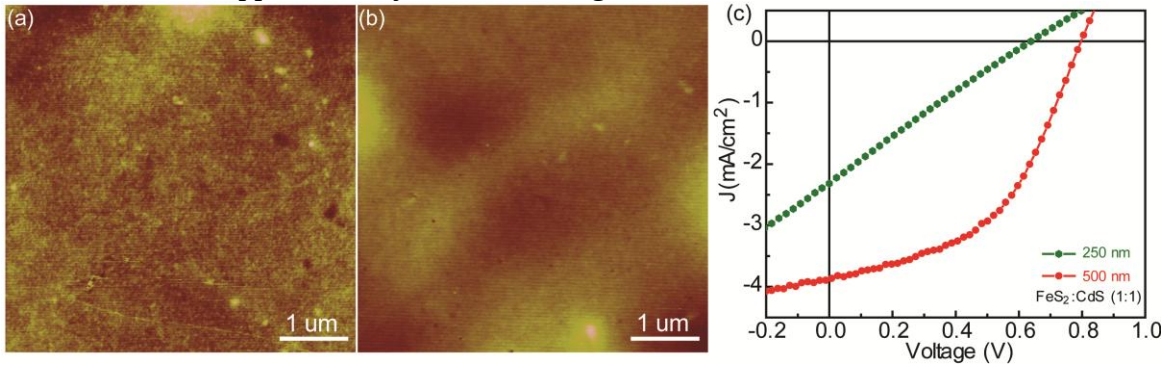

Figure S3. (a) J-V curve of FeS_2 NCs and FeS_2/CdS bi-layer device. (b) SEM cross-sectional image of FeS_2/CdS bi-layer device.

This journal is © The Royal Society of Chemistry 2012

5. J-V Characterization of FeS_2 and CdS NC Schottky and FeS_2/CdS Bi-layer PV Devices.

Figure S4a and S4b show typical current density–voltage (*J–V*) curves obtained from the solar cell devices, prepared with and without the CdS QDs and CdS schottky devices. Al cathodes were used in both cases of Schottky and bi-layer devices, owing to the difference between the work function of Al (ca. 4.3 eV) and the ITO anode (ca. 4.8 eV).[4] The short circuit current (J_{sc}) of CdS schottky device is lower than that of FeS_2/CdS bulk nano-junction structure due to the low photoabsorbance of large bandgap CdS phase. The open circuit voltage (V_{oc}) of CdS schottky device is dictated by the work function difference of electrodes, which is smaller than the band offset between FeS_2 and CdS excitonic interface, resulting a higher V_{oc} in FeS_2/CdS nanojunction device. All these factors contribute to confirm the photoabsorption and photocurrent generation by the incorporation of FeS_2 component, and interfacial heterojunction between electron donor FeS_2 and electron acceptor CdS phases. The cross-sectional SEM image (Figure s3c) of FeS_2/CdS bi-layer device shows the voids existing across the device, which causes the large decrease of PV performance, in comparison with FeS_2/CdS bulk heterojunction solar cells.

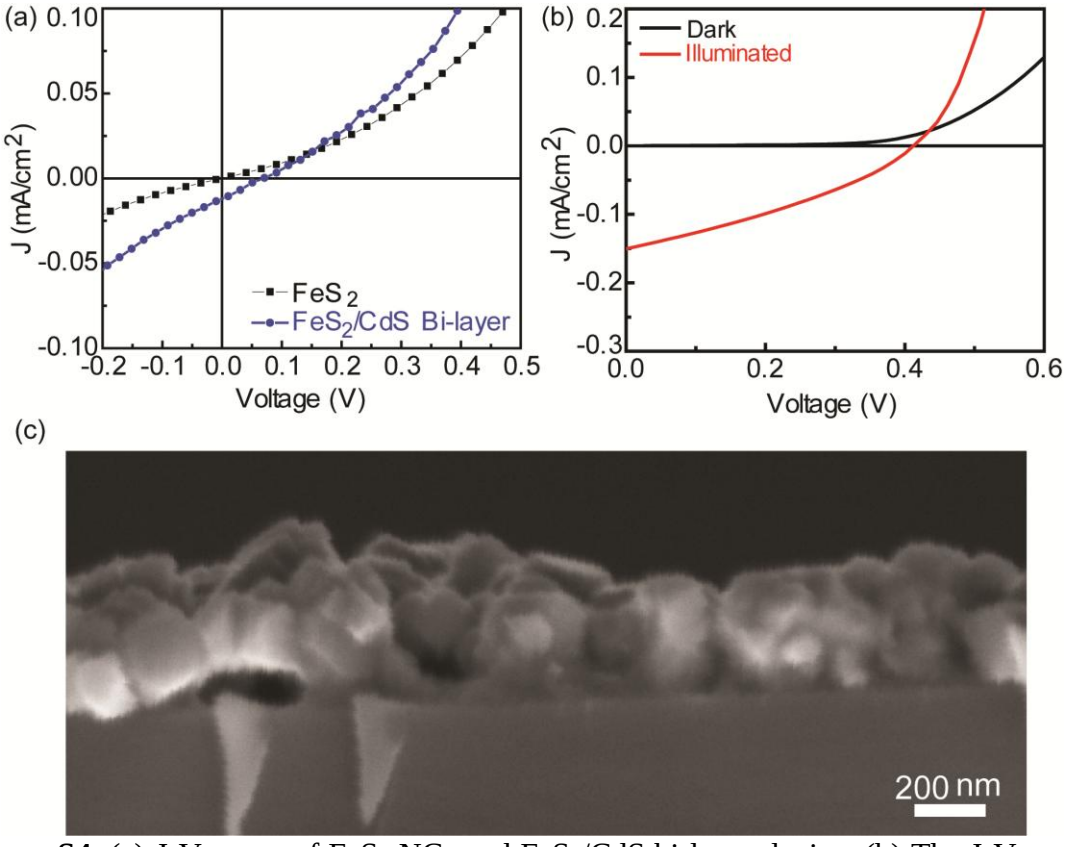

Figure S4. (a) J-V curve of FeS_2 NCs and FeS_2/CdS bi-layer device. (b) The J-V curves of CdS schottky device under dark and illuminated state. (c) SEM cross-sectional image of FeS_2/CdS bi-layer device.

This journal is © The Royal Society of Chemistry 2012

6. NIR LSPRs Photoresponse of FeS_2:CdS BHJ Solar Devices.

The effect of localized surface plasmon resonances (LSPRs) of FeS_2 NCs on the photoelectric properties of FeS_2:CdS films was demonstrated by the DC current density (*J*)–voltage (*V*) characteristics of the BHJ devices under NIR light source (35 mW/cm^2 intensity from 1100-1300 nm wavelength). Near IR light was provided from a xenon light with near IR filter. The power intensity was calibrated by using a Thorlabs PM100D power meter. It should be noted that the LSPRs arising from the noble metal nanocrystals has shown the plasmonic enhanced light absorption via the near field or scattering effect, however, it is very challenging to achieve the direct photoelectric conversion. This is the first time to show the LSPRs based photoelectric effect from the FeS_2 based semiconducting NCs (Figure s5). This opens up a new tactic to enhance the solar light harvesting efficiency.

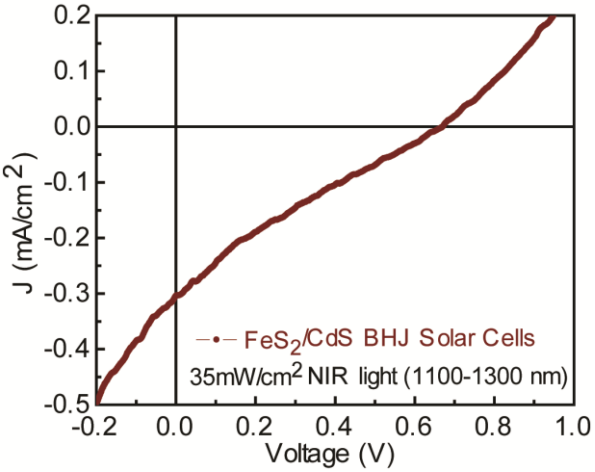

Figure S5. (a) J-V curve of all inorganic FeS_2:CdS BHJ solar device under NIR light illumination to show the direct conversion of LSPRs effect from FeS_2 NCs.

Reference:

[1]Peng, Z. A.; Peng, X. G. *Journal of the American Chemical Society* **2001**, *123*, 183.
[2] Zhao, Y.; Burda, C. *Energy & Environmental Science* **2012**, *5*, 5564.
[3] Puthussery, J.; Seefeld, S.; Berry, N.; Gibbs, M.; Law, M. *Journal of the American Chemical Society* **2010**, *133*, 716.
[4] Zhitomirsky, D.; Kramer, I. J.; Labelle, A. J.; Fischer, A.; Debnath, R.; Pan, J.; Bakr, O. M.; Sargent, E. H. *Nano Letters* **2012**, *12*, 1007.